Journal of Photochemistry and Photobiology A: Chemistry 217 (2011) 299–307

Contents lists available at ScienceDirect

Journal of Photochemistry and Photobiology A: Chemistry

journal homepage: www.elsevier.com/locate/jphotochem

Synthesis, photophysics and excited state structure of 1,8-di(*p*-tolyl)-1,3,5,7-octatetrayne

I. Deperasińska[b], A. Szemik-Hojniak[a], K. Osowska[a], M.F. Rode[b], A. Szczepanik[b], Ł. Wiśniewski[a], T. Lis[a], S. Szafert[a,c,*]

[a] Faculty of Chemistry, University of Wrocław, Joliot-Curie 14, 50-383 Wrocław, Poland
[b] Institute of Physics, Polish Academy of Sciences, Al. Lotników 32/46, 02-668 Warsaw, Poland
[c] Wrocław Research Center EIT+ Ltd., Stabłowicka 147/149, 54-066 Wrocław, Poland

ARTICLE INFO

Article history:
Received 4 June 2010
Received in revised form 8 October 2010
Accepted 26 October 2010
Available online 2 November 2010

Keywords:
Cadiot–Chodkiewicz
Polyynes
Photophysics
Excited state structure
Crystal structure

ABSTRACT

The Cadiot–Chodkiewicz type C_2-elongation of p-tolylacetylene followed by dimerization of the resulted diyne *p*-$CH_3C_6H_4(C{\equiv}C)_2$TMS (**1**) gave thermally stable octatetrayne *p*-$CH_3C_6H_4(C{\equiv}C)_4$-*p*-$C_6H_4CH_3$ (**2**) as light yellow powder in 75% yield. Compound **2** was characterized by spectroscopic methods and X-ray crystallography. Careful analysis of the crystal data revealed high degree of chain linearity with a potential for 1,*n*-topochemical polymerization. Next, photophysical properties of **2** were studied in details by experimental and advanced theoretical methods (*ab initio* HF as well as DFT calculations involving both the ground and excited state geometry optimization). These properties are similar to the properties of the parent polyyne $C_6H_5(C{\equiv}C)_4C_6H_5$ previously described in literature (in particular, the lowest electronic excited singlet state (S_1) of **2** is a dark state). This was confirmed by the experimental facts, namely, few progressions of the stretching mode (a_g) of the polyyne chain, starting from different "false origins" lying below the second excited (bright) state (S_2), were observed in the fluorescence excitation spectrum. The red shift of the electronic spectra (155 cm^{-1} and 300 cm^{-1} for absorption and fluorescence, respectively) and an increase of an energy gap between S_1 and S_2 states by 450 cm^{-1} are the effects of methylation of $C_6H_5(C{\equiv}C)_4C_6H_5$ to **2**. Theoretical results showed that in the excited state of **2** a shortening of single bonds and elongation of triple bonds occurred. This is in accordance with an observation of a long progression of the stretching vibration mode in the experimental absorption spectrum of **2**. Besides that, stretching vibration of the polyyne chain is also active in the fluorescence spectra.

1. Introduction

Long chain organic, organometallic and metal-containing polyynes have attracted a lot of attention within the last two decades. This interest results from high potential of such compounds as nanoscale electronic devices [1] as well as models for carbyne, a yet unknown carbon allotrope [2]. The already synthesized compounds were thoroughly characterized and especially interesting were those with electrochemically active metal end-caps, which enable the compounds to exist in more than one oxidation state [3].

Nevertheless, purely organic polyynes are also being intensively investigated. Many of them occur naturally [4] and have biological activity but they also bear an enormous potential as electronic devices due to their unique electronic and optical properties [5]. From these reasons their photophysical properties are being extensively investigated [6].

Current investigations especially focus on the excited state properties of polyynes in an aim to search for a new type of nanostructural architectures that occur in a form of simple molecular wires or constitute building blocks of more complicated carbon networks [7]. Such architectures may show a nonlinear optical response [8]. Hence, effects of optical excitation in such structures are, in our opinion, extremely important to be recognized [9].

Recently, attention was mostly focused on the systematic observations of changes in absorption and emission spectra of diphenylpolyynes affected by the length of the polyyne chain [9–11]. The character of the fluorescent state was considered in terms of the two lower lying excited states, separated by a small energy gap. One of these two states is optically dark, while the second is a bright one. The photophysical properties of diphenylpolyynes (similarly to other classes of molecules characterized by such a system of states) [12–16] strongly depend on the mutual ordering and the electronic couplings between these two states.

* Corresponding author at: Faculty of Chemistry, University of Wrocław, Joliot-Curie 14, 50-383 Wrocław, Poland. Tel.: +48 71 375 71 22; fax: +48 71 328 23 48.
E-mail address: szaf@wchuwr.pl (S. Szafert).

1010-6030/$ – see front matter © 2010 Elsevier B.V. All rights reserved.
doi:10.1016/j.jphotochem.2010.10.023

In the present work the synthesis, X-ray crystal structure and absorption, emission and excitation emission spectra of 1,8-di(*p*-tolyl)-1,3,5,7-octatetrayne are discussed. The data are compared with those reported by Nagano who described photophysical properties of a series of α,ω-diphenylpolyynes $C_6H_5(C{\equiv}C)_nC_6H_5$ (n = 1–6) [10].

2. Experimental

2.1. Syntheses and characterization

All reactions were conducted under N_2 using standard Schlenk techniques. Solvents were treated as follows: hexane, distilled from Na; CH_2Cl_2 and acetone, distilled from P_2O_5; THF, predried over NaOH and then distilled from Na/benzophenone; $CDCl_3$, vacuum transferred from CaH_2; C_6D_6, vacuum transferred from Na. *p*-$CH_3C_6H_4C{\equiv}CH$ (97%), *n*-BuLi (2.26 M in hexanes), CuCl (99.995+%), CuI (99.999%), $EtNH_2$ (2.0 M in THF), tetramethylethylenediamine (TMEDA; 99%; distilled from NaOH) and tetrabutylammonium fluoride (TBAF; 1.0 M in THF) were obtained from Aldrich and used without further purification unless stated otherwise. $ClSiMe_3$ (Fluka, 99%) was used as received. TMSC≡CI was prepared following the known protocol for related compounds [17].

Infrared spectra were recorded in a KBr cell or in solution on a Bruker 66/s FTIR spectrophotometer. NMR spectra were obtained on a BRUKER ESP 300E and 500 spectrometer. GC–MS analyses were recorded on a gas chromatograph with a mass detector HP 5971A and an infrared detector HP5965B (Hewlett Packard). Microanalyses were conducted with an ARL Model 3410 + ICP spectrometer (Fisons Instruments) and a VarioEL III CHNS (both in-house).

2.2. *p*-$CH_3C_6H_4C{\equiv}CC{\equiv}C$TMS (**1**)

A Schlenk flask was charged with 15 mL of THF and 0.35 mL (2.677 mmol) of 4-ethynyltoluene (*p*-$CH_3C_6H_4C{\equiv}CH$) and cooled to −45 °C. Then 1.30 mL (2.26 M, 2.945 mmol, 1.1 eq.) of *n*-BuLi was added dropwise. After 1 h 0.561 g (2.945 mmol) of CuI was added. The mixture was warmed up to −10 °C. When CuI was completely dissolved temperature was lowered to −45 °C again and 8 mL of $EtNH_2$ and 0.452 mL (2.945 mmol) of TMSC≡CI was slowly added with stirring. After 1 h cold bath was removed and the mixture was stirred at room temperature for another hour. Solvent was evaporated by oil pump vacuum. The residue was dissolved and filtered through a silica gel pad (5 cm, hexanes/CH_2Cl_2, v/v, 10:1). Solvent was removed to give **1** as a yellow-brown thick liquid (85%, 0.483 g, 2.275 mmol).

^{1}H NMR (300 MHz, $CDCl_3$): δ = 7.37 (d, J_{HH} = 8 Hz, 2H, C_6H_4), 7.10 (d, J_{HH} = 8 Hz, 2H, C_6H_4), 2.33 (s, 3H, CH_3), 0.22 (s, 9H, TMS).

IR (cm^{-1}, THF): $\nu_{C{\equiv}C}$ = 2204 vs, 2104 s.

2.3. *p*-$CH_3C_6H_4(C{\equiv}C)_4$-*p*-$C_6H_4CH_3$ (**2**)

A Schlenk flask was charged with 0.220 g (1.036 mmol) of **1** and 10 mL of acetone. The solution was purged with N_2 and wet TBAF (1.0 M solution in THF; 0.21 mL; 0.207 mmol; 20 mol %) was added dropwise. After 20 min 0.13 mL (1.036 mmol) of $ClSiMe_3$ was introduced. After 15 min O_2 was bubbled through the solution for 10 min. In a separate Schlenk flask 0.989 g (10.000 mmol) of CuCl and 0.60 mL of TMEDA (4.000 mmol) were mixed in 5 mL of acetone. A blue supernatant that emerged after 0.5 h was added in portions to the first Schlenk flask. O_2 was bubbled through the reaction. After 4 h solvent was removed by oil pump vacuum. The residue was dissolved in minimum of CH_2Cl_2 and filtered through 10 cm plug of alumina and then through 10 cm plug of celite (washed with hexanes). Solvent was removed by oil pump vacuum. Pale-yellow crystals were obtained from hexanes/CH_2Cl_2 mixture in 75% yield (0.108 g, 0.388 mmol). Product was stored at −20 °C.

^{1}H NMR (300 MHz, C_6D_6): δ = 7.20–6.62 (m, 8H, $2C_6H_4$), 1.87 (s, 6H, $2CH_3$).

$^{13}C\{^1H\}$ NMR (75 MHz, C_6D_6): δ = 133.4, 129.4, 128.3, 118.3 (8C, $2C_6H_4$), 78.7, 74.7, 67.8, 64.7 (4C, C≡CC≡C), 21.4 (2C, $2CH_3$).

EA calc. (%) for $C_{22}H_{14}$ (278.35): C 94.93, H 5.07; found. C 95.03, H 5.01.

IR (cm^{-1}, KBr): $\nu_{C{\equiv}C}$ = 2198 vs, 2094 s.

MS: 278 (M^+).

p.t.t.(I) = 120 °C (nematic); p.t.t.(II) = 156 °C (polymerization).

2.4. Electronic absorption spectra

Electronic absorption spectra in solution were recorded on a CARY-50 UV-VIS (Varian) spectrometer at a concentration of about 10^{-5} M. The solvents used in absorption and emission experiments: 2,2,4-trimethylpentane, methylcyclohexane (MCH), and acetonitrile were of spectroscopic grade and used as purchased (Merck, Uvasol) except for acetonitrile which was dried over the molecular sieves prior to use.

2.5. Steady state emission spectroscopy

Emission spectra were recorded on a FLS920 combined fluorescence lifetime and steady state spectrometer (Edinburgh Instruments Ltd.) using as an excitation source Xe900, 450 W steady state xenon lamp (ozone free) with a computer controlled excitation shutter and spectral bandwidth of ≤5 nm for both excitation and emission spectra. Luminescence was detected using a red sensitive (185–850 nm) single photon counting photomultiplier tube (R928-Hamamatsu) in Peltier cooled housing. For the emission spectra the optical density was kept at ∼0.2 (path length 1 cm) to avoid reabsorption and inner filter effects. Spectra were corrected for detector response and excitation source. The concentration of solutions was about 10^{-5} M. Excitation spectra were corrected for differences in excitation intensity by means of a reference photomultiplier.

2.6. Time-resolved emission spectroscopy

Decay curves were recorded using a nanosecond time-correlated single photon counting (TCSPC) option of FSL920 setup (Edinburgh Instruments Ltd.). Excitation was provided by a nF900 nitrogen filled nanosecond flashlamp under computer control with typical pulses width of 1 ns, pulse repetition rate typically of 40 kHz and possibility of measuring decays from 100 ps to 50 μs. Data acquisition ensured a Plug-in PC Card Model TCC900 with maximum count rate of 3 MHz, time channels per curve up to 4096, and minimum time per channel of 610 fs. A Hamamatsu (R928-Hamamatsu) in Peltier cooled housing was used as detector.

2.7. Theoretical methods

All calculations presented in this work have been performed by ab initio HF and CIS methods as well as by DFT B3LYP and TD-DFT B3LYP in different basis sets (cc-pVDZ and 6-31G(d,p)) in Gaussian 98W [18] and Turbomole [19] packets of programs. The later one permits for excited state optimization by TD-DFT [20] method. For all energy minima, both in the ground and excited state, a full set positive frequency vibrations has been found.

2.8. Details of X-ray data collection and reduction

X-ray diffraction data were collected using a KUMA KM4 CCD (ω scan technique) diffractometer equipped with an Oxford cryosys-

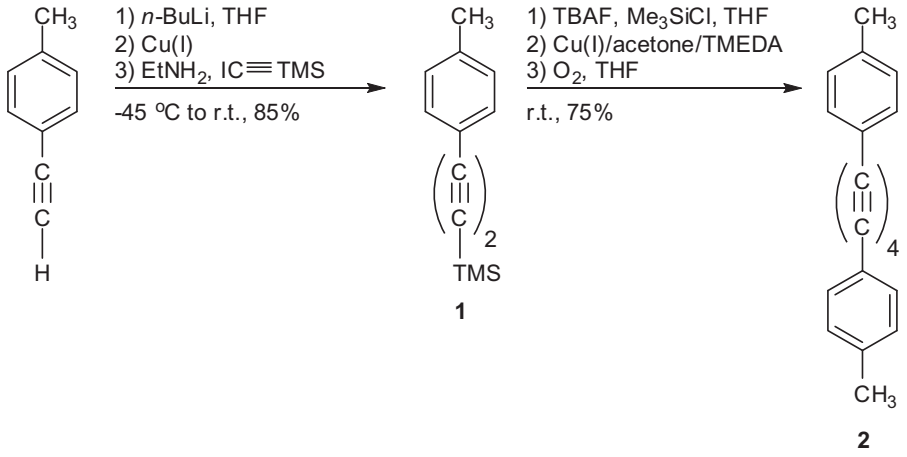

Scheme 1. Synthesis of **2**.

tem cryostream cooler. The space groups were determined from systematic absences and subsequent least-squares refinement. Lorentz and polarization corrections were applied [21]. The structures were solved by direct methods and refined by full-matrix least-squares on *F*2 using the SHELXTL package [22]. Non-hydrogen atoms were refined with anisotropic thermal parameters. Hydrogen atom positions were calculated and added to the structure factor calculations, but were not refined. CCDC-752527 for **2** contains the supplementary crystallographic data for this paper. These data can be obtained free of charge from The Cambridge Crystallographic Data Centre via www.ccdc.cam.ac.uk/data_request/cif.

Table 1
Crystallographic data for **2**.

Complex	**2**
Chemical formula	$C_{22}H_{14}$
Formula weight	278.33
Temp [K]	100 (2)
Space group	C2/c
a [Å]	7.529 (3)
b [Å]	17.983 (8)
c [Å]	11.677 (6)
β [°]	94.73 (5)
V [Å^3]	1575.6 (12)
Z	4
ρ [g/cm^3]	1.173
μ (Mo K$_\alpha$) [mm^{-1}]	0.066
R1 (%) (>2σ)	0.0751
wR2 (%) (>2σ)	0.1298

3. Results

3.1. Synthesis

Synthesis of 1,8-di(*p*-tolyl)-1,3,5,7-octatetrayne followed the already described procedure for other octatetraynes. As shown in Scheme 1 terminal *p*-tolylacetylene was first transformed *via* copper catalyzed Cadiot–Chodkiewicz cross coupling with IC≡CTMS into diyne *p*-$CH_3C_6H_4C{\equiv}CC{\equiv}CTMS$ (**1**) [3g,23]. Workup by column chromatography gave **1** as a yellow–brown thick liquid in 85% yield. One of the obvious approaches to 1,8-di(*p*-tolyl)-1,3,5,7-octatetrayne was deprotection of **1** to terminal diyne *p*-$CH_3C_6H_4C{\equiv}CC{\equiv}CH$ (**3**) and then its oxidative homocoupling. In order to avoid isolation and purification of terminal diyne **3** which, as many others, could appear unstable, we decided to proceed with a protocol that includes *in situ* deprotection that is immediately followed by addition of $ClSiMe_3$ (as an F^- ion scavenger) and then CuCl/TMEDA/O_2 system for oxidative homocoupling [3i,24]. Reaction workup on alumina and celite resulted in yellow powder which was recrystallized from a mixture of hexanes/CH_2Cl_2 to yield pale-yellow crystals of **2** in 75% yield.

Compounds **1** and **2** were characterized by IR and ^{1}H NMR spectroscopy which were routine. Their IR spectra (KBr) showed two $\nu_{C\equiv C}$ bands at 2204 (vs) and 2104 (s) cm^{-1} for **1** and at 2198 (vs) and 2094 (s) cm^{-1} for **2**. The ^{1}H NMR spectra revealed signals of the diagnostic CH_3 group at δ = 2.33 and 1.87 ppm for **1** and **2**, respectively. Spectrum of **1** exhibited also the signal of TMS group at 0.22 ppm. The ^{13}C NMR of **2** showed a signal of the CH_3 carbon at 21.4 ppm and four signals of the chain carbon atoms at 78.7, 74.7, 67.8, and 64.7 ppm. Its mass spectrum showed an intense parent ion (100%) and gave correct microanalysis. The compound also showed phase transformation after melting at 120 °C to nematic phase and then polymerized at 156 °C.

3.2. X-ray crystal structure

The crystal structures of **2** was determined as outlined in Table 1 and described in Section 2. A view of the molecule is presented in Fig. 1.

The molecule lies at the two-fold axis what enables a twist of the two phenyl rings by 19.7°. The bond lengths within the carbon chain are 1.216(3) and 1.218(3) Å for the triple bonds C(1)≡C(2) and C(3)≡C(4) and 1.361(3) and 1.358(4) Å for the single bonds

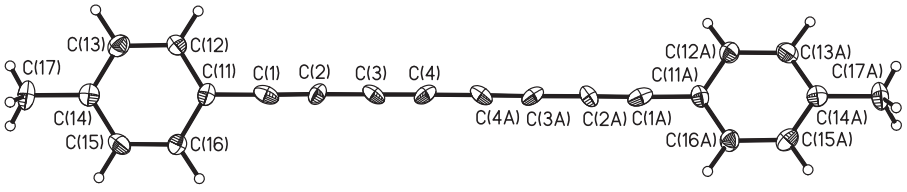

Fig. 1. View of **2**. Selected bond lengths (Å) and angles (°): C(1)–C(11) 1.434(3), C(1)–C(2) 1.216(3), C(2)–C(3) 1.361(3), C(3)–C(4) 1.218(3), C(4)–C(4A) 1.358(4), C(11)–C(1)–C(2) 179.4(3), C(1)–C(2)–C(3) 179.1(3), C(2)–C(3)–C(4) 178.9(2), C(3)–C(4)–C(4A) 179.43(15).

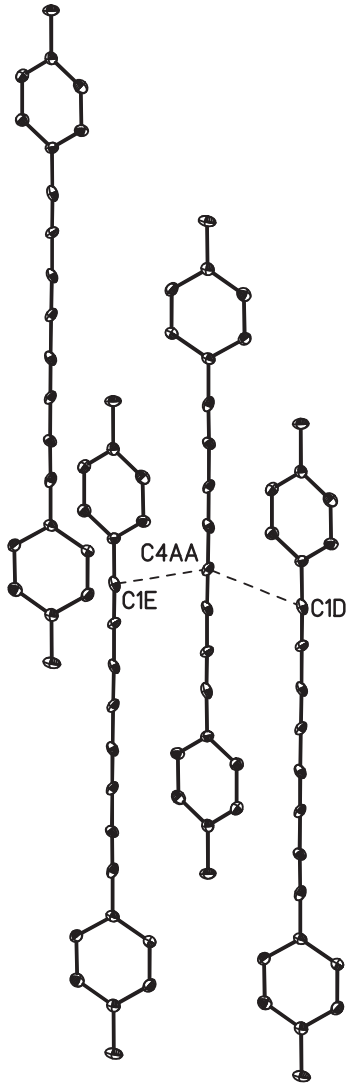

Fig. 2. Example of a packing diagram for **2**. Packing parameters: closest chain–chain contact 4.168 Å, φ = 18.1°, offset distance = 11.099 Å, fractional offset = 0.94. Distances for potential 1,4-topochemical polymerization: C4AA-C1D 4.893 Å; C4AA-C1E 5.056 Å.

C(2)–C(3) and C(4)–C(4A). These values are typical and are similar to those observed for other tetraynes [25].

Although C_8 chains are long enough to perform a distinctive deformation the one in **2** shows high degree of linearity as evidenced by the close correspondence of the C(11)–C(11A) distance (11.813 Å) with the sum of all the bond lengths within the carbon chain (11.816 Å) corresponding to the contraction of 0.0% [25,26]. High degree of linearity is also nicely "visualized" by the high average value of the chain C–C–C bond angles of 179.1°.

Next a potential of **2** for the 1,*n*-topochemical crystal-to-crystal polymerization was established. The compound **2** crystallizes in the monoclinic system in the C2/c space group. As a consequence, its molecules pack to form one set of parallel chains as shown in Fig. 2. First the closest chain–chain separation was analyzed [25]. Although the endgroups are not particularly bulky it appeared to be 4.168 Å, which is higher than the sum of Van der Waals radii (3.56 Å). The distance is associated with φ angle and an offset value (a measure of the mutual position of neighboring chains) of 18.1° and 11.099 Å (fractional offset 0.94), which is not far off from the value for an ideal candidate for the 1,8-topochemical polymerization (optimum geometrical conditions are: φ angle = ca. 21°,

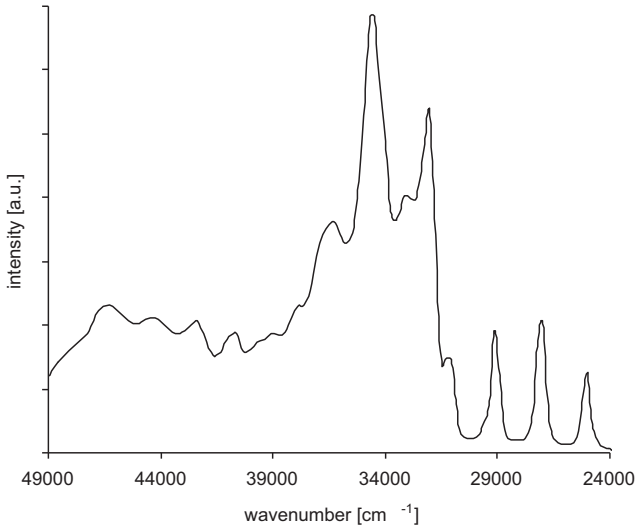

Fig. 3. Absorption spectrum of **2** in methylcyclohexane.

carbon–carbon distance = ca. 3.5 Å). The slightly longer distances that are associated with atom positioning for 1,4-topochemical polymerization are larger and equal 4.893 Å (C4AA-C1D) and 5.056 Å (C4AA-C1E). The packing parameters for **2** are summarized in Fig. 2 caption.

3.3. *Absorption, excitation fluorescence, and fluorescence spectra*

The spectral characteristics of **2** are given in Figs. 3 and 4. They show its room temperature absorption spectrum and the low temperature (77 K) fluorescence and excitation fluorescence spectra in methylcyclohexane. It was also established that **2** does not exhibit any solvatochromic effect and in both apolar 2,2,4-trimethylpentane or strongly polar acetonitrile presents similar features.

All these spectra of **2** are only slightly different from those for $C_6H_5(C{\equiv}C)_4C_6H_5$ [10]. Thus, due to methylation, the maximum of absorption (24,955 cm^{-1}) and fluorescence (20,160 cm^{-1}) bands of

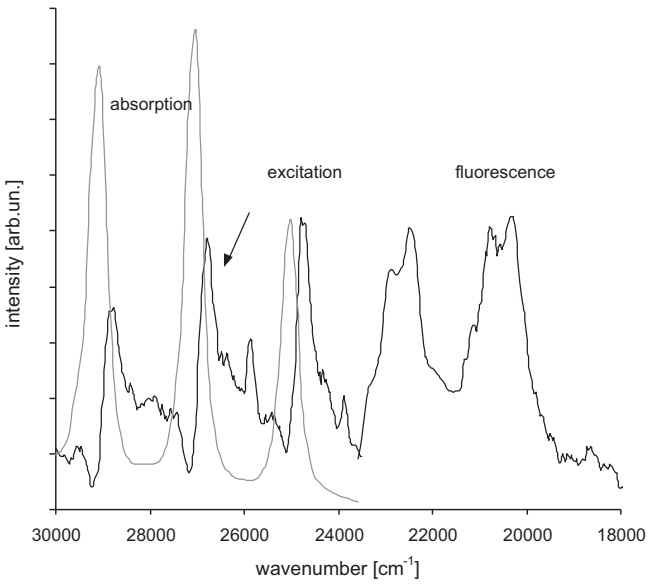

Fig. 4. Low temperature (77 K) fluorescence (exc = 400 nm) and excitation fluorescence spectra (exc = 400, em = 455 nm) of **2** in methylcyclohexane. For comparison, the room temperature absorption spectrum (part of spectrum in Fig. 3) is also presented.

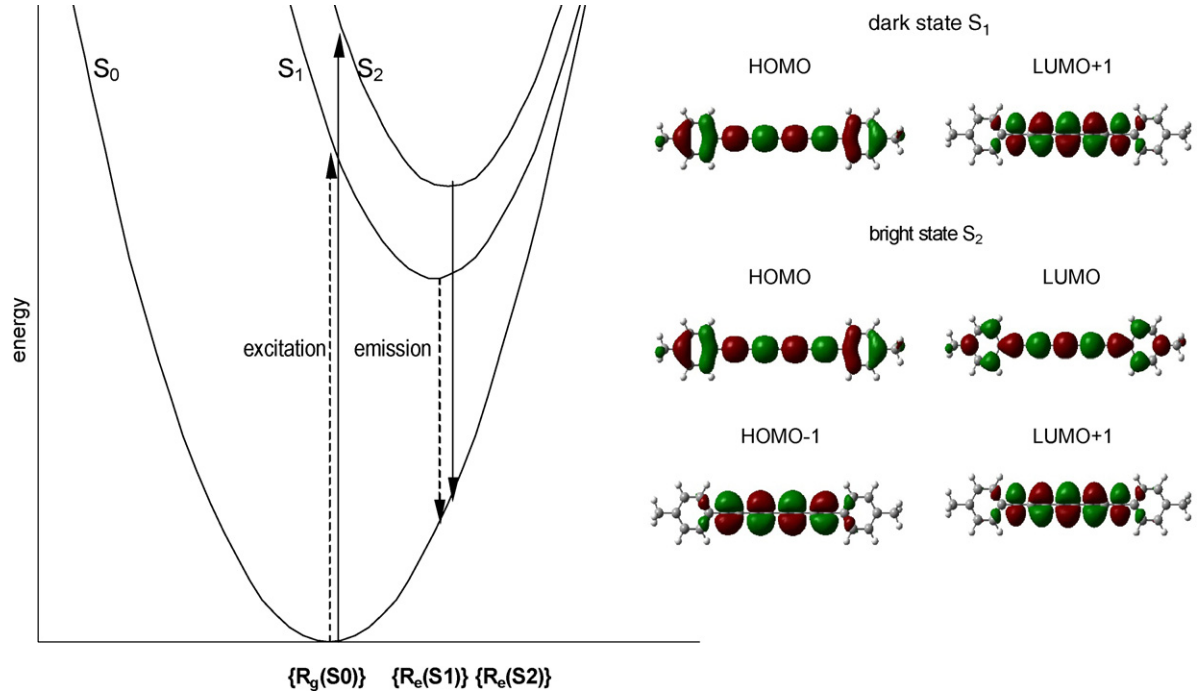

Fig. 5. Potential energy surfaces of **2** in its ground and electronic excited states (left) together with electronic configurations that contribute to its two lowest excited electronic (right). $\{R_i(S_k)\}$ represents the set of geometry parameters for energy minimum in k-th electronic state with $k = S_0, S_1, S_2$. One may notice, that $\{R_g(S_0)\}$ corresponding to the energy minimum of S_0 is clearly different from those of $\{R_e(S_1)\}$and $\{R_e(S_2)\}$. Besides that, the both $\{R_e(S_1)\}$ and $\{R_e(S_2)\}$ sets, corresponding to the minima of energy in the excited states, are similar. The dashed arrows characterize the forbidden transitions.

2 are blue shifted by about 155 cm^{-1} and 300 cm^{-1}, respectively, compared to $C_6H_5(C{\equiv}C)_4C_6H_5$. In excitation fluorescence spectra, there are only slight differences between the maxima of both systems (~20–80 cm^{-1}) and similarities are mainly concerned with band structure and intensity distribution.

Peak spacing in the absorption band of **2** is 2035 cm^{-1} relative to 2050 cm^{-1} in $C_6H_5(C{\equiv}C)_4C_6H_5$ whereas in the fluorescence spectra these values are 2136 cm^{-1} and 2150 cm^{-1}, respectively. Finally, in the low temperature excitation fluorescence spectrum of **2**, vibration of 2050 cm^{-1} in comparison to 2080 cm^{-1} for $C_6H_5(C{\equiv}C)_4C_6H_5$ is observed. These frequencies are assigned to the symmetric stretching modes of polyyne chain for excited and ground states of polyynes. Likewise in $C_6H_5(C{\equiv}C)_4C_6H_5$, no mirror symmetry image between excitation fluorescence and the fluorescence spectra of **2** is observed.

In the discussion of experimental results obtained for $C_6H_5(C{\equiv}C)_4C_6H_5$ [10], a model with two closely lying excited states: dark ^1A and bright $^1B_{1u}$ was proposed. Semiempirical formula adapted there has been derived from the free electron theory for a one-dimensional box [27].

In the present work, we verify this model on the basis of computational results that we have obtained using more advanced quantum-chemical calculations involving not only the ground state optimization but also excited state optimization of **2**.

3.4. Theoretical calculations

3.4.1. General characteristics

The calculations involving the ground state optimization (S_0 state) and excited state optimization of the two lower-lying electronic excited states (S_1, S_2) both for **2** and $C_6H_5(C{\equiv}C)_4C_6H_5$ molecules have been performed using *ab initio* HF and DFT method in few typical basis sets. We started our calculations without any indication of the symmetry of **2** and the results showed the molecule to have C_1 symmetry. However in practice the molecular orbitals and other properties of **2** are very similar to those for $C_6H_5(C{\equiv}C)_4C_6H_5$ with D_{2h} symmetry. The results for $C_6H_5(C{\equiv}C)_4C_6H_5$ molecule are not presented here, because – similarly as the experimental results – they are very similar to the results for **2** and were used only for comparison. In particular, the comparison of calculated vibration modes for $C_6H_5(C{\equiv}C)_4C_6H_5$ (as the molecule of higher symmetry than **2**) with vibration modes calculated for **2** was used for identification of b_{1g} type modes which act as coupling modes between two lowest electronic excited states.

Excited state optimization aimed to establish the changes of molecular geometry of **2** in its electronic excited states in comparison to the ground state and how the mutual energetic ordering of its optimized excited states looks like.

The calculated potential energy surfaces for **2** are qualitatively presented in Fig. 5 (a more detailed data will be given in Tables 2–4). This picture is common for the *ab initio* HF and DFT calculations. It demonstrates that large differences in molecular geometry exist between molecule in the ground S_0 state (denoted symbolically as $\{R_g(S_0)\}$) and in the excited S_1 and S_2 states (denoted as $\{R_e(S_1)\}$ and $\{R_e(S_2)\}$) while differences between the molecular geometries corresponding to both considered excited states are rather small.

Table 2
The ground state (S_0) interatomic distances in polyyne chain calculated by DFT B3LYP/cc-pVDZ and HF/cc-pVDZ methods in comparison to the experimental data (see Fig. 1).

Pair of atoms in polyyne chain (for labels see Fig. 1)	Interatomic distances in [Å]		
	Experiment	Calculation results	
		DFT	HF
C(1)–C(11)	1.434	1.421	1.439
C(1)–C(2)	1.216	1.230	1.198
C(2)–C(3)	1.361	1.354	1.383
C(3)–C(4)	1.218	1.236	1.200
C(4)–C(4A)	1.358	1.348	1.380

Table 3
The calculated bond lengths in polyyne chain of **2** in the ground state (R_g) and in the excited electronic state (R_e) and differences between them ($\Delta R = R_e - R_g$). The calculations are performed by DFT and TD DFT B3LYP/cc-pVDZ, HF and the CIS/cc-pVDZ methods. All lengths are given in [Å].

Pair of atoms in polyyne chain (for labels see Fig. 1)	DFT and TD DFT B3LYP			HF and CIS		
	R_g	R_e	ΔR	R_g	R_e	ΔR
C(1)–C(11)	1.421	1.410	−0.011	1.439	1.429	−0.010
C(1)–C(2)	1.230	1.257	0.027	1.198	1.222	0.024
C(2)–C(3)	1.354	1.315	−0.039	1.383	1.335	−0.048
C(3)–C(4)	1.236	1.286	0.050	1.200	1.259	0.059
C(4)–C(4A)	1.348	1.296	−0.052	1.380	1.306	−0.074

It is also noted (by doted arrows) that the optical transition to the S_1 excited state is forbidden (and therefore it is a dark state). However, in reality, due to the coupling between electronic states, such transitions are possible and observed [12–16].

Electronic configurations describing the two excited states (S_1 and S_2) of **2** are illustrated also in Fig. 5. One may easily notice that they result from excitation between the two highest occupied (HOMO-1 and HOMO) and two lowest unoccupied (LUMO and LUMO+1) molecular orbitals. Despite that all of them are of the π-type orbitals, they are lying in two perpendicular molecular planes and correspond to b_{3g}, b_{2g}, b_{3u} and b_{2u} orbitals in D_{2h} group of symmetry for unmethylated diphenylpolyynes [9–11]. As is seen from Fig. 5, the dark S_1 state is the result of an electron transition between the $b_{2g} \rightarrow b_{2u}$ orbitals, whereas the bright S_2 state results from excitation between $b_{3g} \rightarrow b_{2u}$ and $b_{2g} \rightarrow b_{3u}$ orbitals These two states correspond to the ^1A_u and $^1B_{1u}$ states in D_{2h} group of symmetry for unmethylated diphenylpolyynes [9–11]. It is known that the coupling between states of such symmetry can be induced by vibrations of b_{1g} type symmetry [12–16].

3.4.2. Optimized geometries

The more detailed calculation results for the ground and excited state geometry of the polyyne chain in **2** are presented in Tables 2 and 3. In Table 2, a comparison between the ground state calculated and experimental bond lengths obtained in this work (see Fig. 1) is presented. This comparison shows that the calculations nicely reproduce the experimental data for interatomic distances in polyyne chain of **2** and that the bond lengths calculated by the DFT method are closer to experimental values than those calculated by the HF method. The calculated angle between the two phenyl rings is practically equal to zero, while in the crystal it is about 20°. Such the difference might be related to packing effect in the crystal of **2**.

Table 3 illustrates the geometry differences between the ground state and the excited states (the calculated geometry parameters for both excited states are quite resembling and differences do not exceed 0.004 Å).

Generally, it is clear from the results presented in Table 3 that geometry differences between the ground and excited state are significant. One should notice that in electronic excited states of **2**, a shortening of single bonds and elongation of triple bonds takes place. According to calculations results, these changes are so large, that in the framework of DFT method the triple bond C(3)–C(4) becomes almost equal to the single bond C(4)–C(4A) (see Table 3 for details). Such result is intriguing and it requires further experimental investigations. Presently, some estimations can be obtained from the analysis of vibrational structure of the absorption band.

In the first absorption band of **2**, likewise in other polyynes [9–11] only a single frequency progression of 2050 cm^{-1} is visible. This frequency is assigned to the symmetric stretching mode of polyyne chain for excited **2**. Intensity ratio of successive components of such progression is governed by Franck–Condon factors [9,16,28]. For example, for the transition from lowest ($w = 0$) vibrational level in the ground electronic state to vibrational level v in the excited electronic state Franck–Condon factor is given as:

$$FC(0, v) = | < 0|v > |^2 = (v!)^{-1} \left(\frac{\Delta^2}{2}\right)^v \exp\left(-\frac{\Delta^2}{2}\right)$$

where Δ is the dimensionless normal mode displacement [28]. For **2** this factor obtained on the basis of intensity ratio in the absorption spectra (shown in Fig. 3) is 1.82.

From theoretical point of view Δ depends on the differences in molecular geometry between the two states involved in the transition and may be determined as a projection of geometry changes between the two states participating in the electronic transition on the normal modes of the excited state [28,29]. In Fig. 6, results of such calculations for all modes of **2** are presented.

As can easily be seen, only some of vibrations of molecule are characterized by Δ parameter of the value that is larger than zero. Frequencies of these vibrations can be observed in the vibration structure of the absorption spectrum. It is also evident from Fig. 6 that parameter Δ for vibration at 2050 cm^{-1} is definitely the largest one. Hence, according to the results of calculations this mode should dominate in the spectra. Actually, this finding well agrees with the experiment and this mode dominates not only in the spectrum of **2** but also in spectra of other polyynes [9–11]. Observation of vibronic structures associated with other vibrations (with a smaller Δ values) requires a change of experimental conditions for registration of better resolved spectra. However, the calculated value of Δ parameter for 2050 cm^{-1} is larger than the experimentally determined one what may denote that the real dif-

Table 4
Transition energies and oscillator strengths calculated for excitation and emission of fluorescence of **2** (calculations by TDDFT B3LYP/cc-pVDZ and CIS/cc-pVDZ methods).

Transition	TD DFT B3LYP		CIS	
	ΔE [eV]	f	ΔE [eV]	f
$S_0 \rightarrow S_1$	2.741	0.000	3.925	0.000
$S_0 \rightarrow S_2$	2.754	0.458	4.055	0.280
$S_1 \rightarrow S_0$	2.338	0.000	2.723	0.000
$S_2 \rightarrow S_0$	2.412	0.413	2.972	0.155

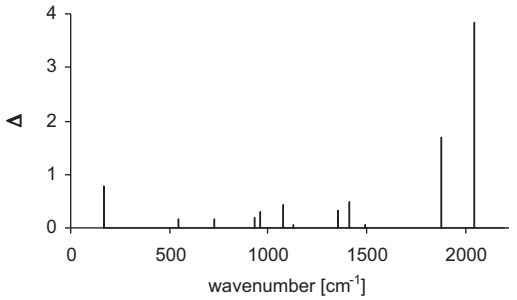

Fig. 6. Dimensionless normal mode displacement of **2** for particular modes in its excited state calculated on the basis of results obtained by means of HF and RCIS/cc-pVDZ method. Frequencies of vibrations are given with the scaling factor of 0.849 (for details see Table 5).

Table 5
Experimental and calculated frequencies of the stretching mode of the polyyne chain of **2** that was used for determination of scaling factor for the calculated frequencies and the re-scaled, on this basis, calculated frequencies of its b_{1g} mode.

	Ground state		Excited state	
	exp.	cal.	exp.	cal.
A. Calculations of scaling factor				
$(-C\equiv C-)_4$ vibration (a_g)	2136	2560	2050	2414
scaling factor = ν_{cal}/ν_{exp}	0.823		0.849	
B. Calculated and rescaled frequencies for modes which couple S_1 and S_2 states				
	382		399	
	815		838	
	956		985	

ferences between geometry of the excited and the ground state are smaller than calculated and shown in Table 3.

3.4.3. Electronic transition energies

Detailed results of the calculations of the excitation and emission energies for **2** are collected in Table 4.

Comparison of the calculation results to the experimental data needs carefulness (see further discussion) but in general the energy for allowed $S_0 \rightarrow S_2$ transitions calculated by RHF method is about 0.8 eV higher compared to the experiment (~3.1 eV) while that by DFT method is about 0.35 eV lower. In turn, analogical comparison for emission from the excited state favors the results of ab initio method (2.8 eV with respect to the experimental values of about 2.85 eV) over the DFT (~2.4 eV).

Such discrepancies of the calculated values of electronic transition energies, by means of different computational methods, have also been found in the literature for the shorter polyynes [9]. This is not, however, the problem of polyynes themselves because, generally, it is known that energy calculations for electronic transitions still constitute a problem in quantum chemistry [30–32].

3.4.4. Some results for vibrations of **2**

As we mentioned previously the experimental spectra of **2** are structured with symmetric stretching mode of polyyne chain. These data can serve determination of so-called "scaling factor" which permits the recalculation of theoretically determined frequencies of vibration with respect to the experimental values. This is done in part A of Table 5.

From the point of view of goals of this work it was needed to indicate frequencies of modes which act as coupling modes for S_1 and S_2 electronic excited states. In part B of Table 5 we give frequencies of such modes of **2**. They are found by comparison with the calculated b_{1g} modes in calculations performed for $C_6H_5(C\equiv C)_4C_6H_5$ and rescaled by factors done in part A of Table 5.

4. Discussion of results

4.1. Excitation fluorescence spectra

More details on vibrational structure of the $S_0 \rightarrow S_1$ transition are revealed in the low temperature excitation fluorescence spectra of **2**.

Fig. 7 and Table 6 demonstrate that besides the single clear progression at 2050 cm^{-1} (indicated in Fig. 7 as D) mentioned already in the absorption spectrum, two other progressions (A and B) of the same mode but at lower energies than the progression D may be distinguished. Somewhat less clear is progression C. In below mentioned analysis no interpretation is suggested for this one. The point is that this progression consists of the broad bands (see Fig. 7) with rather diffused maxima and one may treat it rather as a contribution from different combinations of the coupling modes.

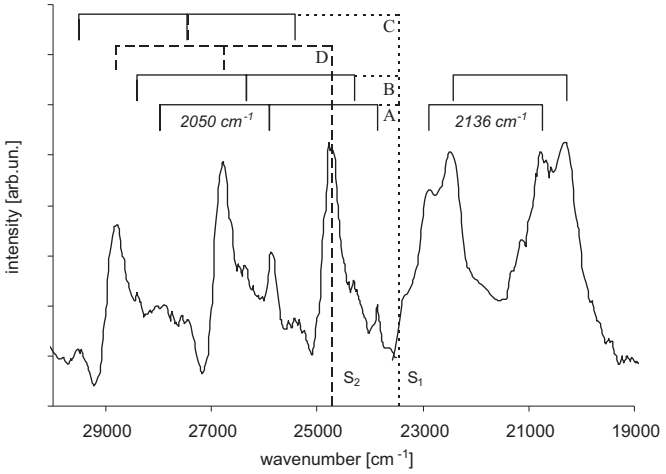

Fig. 7. Excitation fluorescence spectra and fluorescence spectra of **2** with distinguished progressions A, B, C corresponding to vibronic transitions to the dark state S_1 together with progression D corresponding to vibronic transitions to the bright state S_2. Details connected with these assignments and with position of S_2 state are given in Table 6.

The excitation fluorescence spectrum is a typical picture for a system with a dark excited state lying below a bright one [13,15,16], where the vibronic coupling between these two states takes place. Due to this coupling, the transitions from the ground state to the dark state are observed as starting from the so-called "*false origin*" in which the electronic energy of the dark state is increased about the frequency of the coupling mode (see Fig. 7 and Table 6).

It results from analysis given in Fig. 7 and Table 6 that we may locate the dark state (S_1) at about 23,465 cm^{-1}. This state is coupled with bright S_2 state by two vibrations at 401 and 836 cm^{-1}. The frequencies of these vibrations are in accordance with calculated frequencies of b_{1g} type vibrations for **2**, namely: 399 and 838 cm^{-1} (compare Table 5).

Hence, the separation between the S_1 and S_2 states could be estimated for about 1260 cm^{-1} (~0.16 eV) and due to methylation is larger about 450 cm^{-1} in comparison to the energy gap for the parent $C_6H_5(C\equiv C)_4C_6H_5$ [10]. It can also be noted that separation of 0.16 eV is comparable to 0.13 eV predicted for **2** by CIS method and slightly larger than 0.013 obtained with TDDFT method (see Table 4).

Table 6
Experimental data and interpretation of excitation fluorescence spectra of **2**. The subsequent entries from the right side indicate as follows: the number of excited state; experimental band position; interpretation of component position in progression; divergence between experimental and assigned frequency; frequency of the coupling mode; labels for particular progressions used in Fig. 7.

State	Exp. band	Description	δ	Coupling mode	
S_1	**23,465**				A
	23,866			$h\nu_1 = 401\ cm^{-1}$	
	25,906	23,866 + 1 × 2050	10		
	27,972	23,866 + 2 × 2050	−6		
	24,301			$h\nu_2 = 836\ cm^{-1}$	B
	26,350	24,301 + 1 × 2050	1		
	28,409	24,301 + 2 × 2050	−8		
	25,412			$?h\nu_3 = 1947\ cm^{-1}$	C
	27,462	25,412 + 1 × 2050	0		
	29,512	25,412 + 2 × 2050	0		
S_2	**24,722**				D
	26,773	24,722 + 1 × 2050	−1		
	28,818	24,722 + 2 × 2050	4		

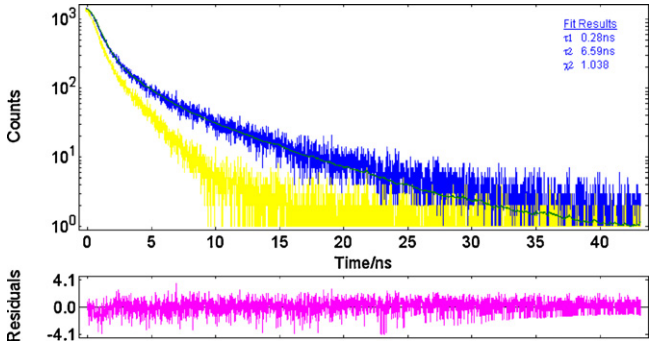

Fig. 8. Bi-exponential decay curve of **2** in 3MP at room temperature (exc = 400 nm, em = 455 nm) [τ_1 = 0.28 ns (82%); τ_2 = 6.59 ns (18%); χ^2 = 1.038].

4.2. Fluorescence spectrum

Like excitation spectra, the fluorescence spectra of the molecule possessing the lowest dark state vibronically coupled with its higher bright state is built up on progressions starting from different coupling modes [15].

One should realize that the fluorescence spectra of **2** are difficult to interpret because among all present bands only two are well defined and separated one from another by about 2136 cm^{-1}. This frequency is undoubtedly connected with the ground state stretching vibration of the polyyne chain and one has to keep in mind that, both in experiment and in calculations, it is higher than its excited state frequency (see Table 5).

Hence, in the fluorescence spectra, like excitation fluorescence spectra of **2**, progression of this mode starting from different coupling modes is observed. Besides that, on each of these two well defined bonds, traces of vibrational structure in the form of two peaks separated by about 425 cm^{-1} are visible. There is, however, too small a number of data for a similar analysis that was performed in the case of excitation fluorescence spectrum.

Comparison of the fluorescence spectra of **2** and $C_6H_5(C{\equiv}C)_4C_6H_5$ [10,11], shows a very similar vibrational structure although the spectra of the former are more diffused. For this reason it is difficult to estimate whether a blue shift of about 300 cm^{-1} in the spectra of **2** relative to $C_6H_5(C{\equiv}C)_4C_6H_5$ is a real fact or whether it may be assigned to diffusion effects or even to a sort of an *arty-fact*.

On the other hand, comparison of the fluorescence spectra of $C_6H_5(C{\equiv}C)_4C_6H_5$ in methylocyclohexane [10], with its spectra in PMMA matrices [11] shows that the latter ones are blue shifted of about 200–500 cm^{-1}. Additionally, it shows that in electroluminescence spectra of $C_6H_5(C{\equiv}C)_nC_6H_5$, some of vibrational components disappear. It means that while referring it to our fluorescence spectrum, displayed in Fig. 7, disappearance of one of the two visible progressions may also be expected.

The authors of the latter work [11] interpret the obtained results as a proof of two fluorescent states being present in $C_6H_5(C{\equiv}C)_4C_6H_5$. One has to keep in mind, however, that the couplings between closely lying states are extremely sensitive to the energy gap between both of them. Hence, disappearance of one of the two progressions may also be caused by a weakening of the coupling interactions in one of the modes.

It seems that in order to solve these problems, the fluorescence spectra with more visible vibrational structure and the lifetimes of particular structural components are required. Experimental lifetimes in acetonitrile, demonstrated in Fig. 8, show two components in the excited state: τ_1 = 0.28 ns (82%); τ_2 = 6.59 ns (18%).

We may assign them to the structure of two different conformers of **2** resulting from rotation around the single C–C bond in the excited state. For example, it is suggested that diphenyldiacetylene in liquid solution exists as a mixture of rotational isomers, one with a planar and the other with a non-planar molecular conformation [33].

5. Summary

In this work, synthesis, characterization including X-ray crystal structure and analysis of absorption, excitation fluorescence and fluorescence spectra of 1,8-di(*p*-tolyl)-1,3,5,7-octatetrayne has been discussed. Data showed that the compound can easily be synthesized by using standard procedures for carbon chain elongation (Cadiot–Chodkiewicz coupling) and oxidative coupling of terminal acetylenes. Photophysical results, complemented by the quantum mechanical calculations have shown that: (1) observation of a long progression of the stretching vibration mode in experimental absorption spectrum of **2** agrees with theoretical result that in the excited state a shortening of single bonds and elongation of triple bonds may occur (the size of those changes are the matter of explanation); (2) the lowest electronic excited state in **2** is a dark state. This theoretical result is confirmed by the experiment, namely by the observation of characteristic excitation fluorescence spectrum with few progressions of vibration frequencies starting from the "false origins", lying below the bright state. On this base the separation between dark and bright states was estimated; (3) both in excitation fluorescence and in the fluorescence spectra, the most active is the stretching vibration of the polyyne chain. Better resolved excitation fluorescence spectra and the fluorescence spectra should answer the question whether, accordingly to theoretical results, a similar role is played by some other modes.

It would be interesting, among other future studies on **2** and related compounds, to start with manipulation of the energy gap between its two lower lying excited states and due to different substitutents in the phenyl rings to generate the CT states, as the electron may jump through bonds as through electric wire.

Acknowledgements

The authors would like to thank the Polish Ministry of Science and Higher Education (Grants: N204 140 31/3236 and N N204 131338) for support of this research. Computations were performed in the Interdisciplinary Center of Mathematical and Computer Modeling (ICM) of Warsaw University in the framework of computational grant Nr G-32-10.

References

[1] (a) Y. Hoshino, Platinum Met. Rev. 45 (2001) 2;
(b) T.M. Swager, C.J. Gil, M.S. Wrighton, J. Phys. Chem. 99 (1995) 4886;
(c) Y. Hoshino, S. Higuchi, J. Fieldler, C. Su, A. Knödler, B. Schwederski, B. Sakar, H. Hartmann, W. Kaim, Angew. Chem. Int. Ed. 42 (2003) 674;
(d) V. Grosshenny, A. Harriman, R. Ziessel, Angew. Chem. Int. Ed. Eng. 34 (1995) 1100;
(e) R.W. Wagner, J.S. Lindsey, J. Am. Chem. Soc. 116 (1994) 9759;
(f) J.S. Schumm, D.L. Pearson, J.M. Tour, Angew. Chem. Int. Ed. Eng. 33 (1994) 1360.
[2] (a) P.P.K. Smith, P.R. Buseck, Science 216 (1982) 984;
(b) Y.P. Kudryavtsev, S. Evsyukov, M. Guseva, V. Babaev, V. Khvostov, in: P.A. Thrower (Ed.), Chemistry and Physics of Carbon, vol. 25, Marcel Dekker, New York, 1997, pp. 1–69;
(c) F. Cataldo, Polym. Int. 44 (1997) 191;
(d) R.J. Lagow, J.J. Kampa, H.-C. Wei, S.L. Battle, J.W. Genge, D.A. Laude, C.J. Harper, R. Bau, R.C. Stevens, J.F. Haw, E. Munson, Science 267 (1995) 362.
[3] (a) A. Sakurai, M. Akita, Y. Moro-oka, Organometallics 18 (1999) 3241;
(b) M. Akita, M.-C. Chung, A. Sakurai, S. Sugimoto, M. Terada, M. Tanaka, Y. Moro-oka, Organometallics 16 (1997) 4882;
(c) A.B. Antonova, M.I. Bruce, B.G. Ellis, M. Gaudio, P.A. Humphrey, M. Jevric, G. Melino, B.K. Nicholson, G.J. Perkins, B.W. Skelton, B. Stapleton, A.H. White, N.N. Zaitseva, Chem. Commun. (2004) 960;
(d) S. Rigaut, J. Perruchon, L. Le Pichon, D. Touchard, P.H. Dixneuf, J. Organomet. Chem. 670 (2003) 37;
(e) H. Qi, A. Gupta, B.C. Noll, G.L. Snider, Y. Lu, C. Lent, T.P. Fehlner, J. Am. Chem. Soc. 127 (2005) 15218;

(f) M.I. Bruce, B.D. Kelly, B.W. Skelton, A.H. White, J. Organomet. Chem. 604 (2000) (150, and references therein);
(g) R. Dembinski, T. Bartik, B. Bartik, M. Jaeger, J.A. Gladysz, J. Am. Chem. Soc. 122 (2000) 810;
(h) G.-Y. Xu, G. Zou, Y.-H. Ni, M.C. DeRosa, R.J. Crutchley, T. Ren, J. Am. Chem. Soc. 125 (2003) 10057;
(i) W. Mohr, J. Stahl, F. Hampel, J.A. Gladysz, Chem. Eur. J. 9 (2003) 3324;
(j) J. Stahl, J.C. Bohling, E.B. Bauer, T.B. Peters, W. Mohr, J.M. Martín-Alvarez, F. Hampel, J.A. Gladysz, Angew. Chem. Int. Ed. 41 (2002) 1871;
(k) G.R. Owen, J. Stahl, F. Hampel, J.A. Gladysz, Organometallics 23 (2004) 5889;
(l) J. Stahl, W. Mohr, L. de Quadras, T.B. Peters, J.C. Bohling, J.M. Martín-Alvarez, G.R. Owen, F. Hampel, J.A. Gladysz, J. Am. Chem. Soc. 129 (2007) 8282.
[4] R.R. Tykwinski, A.L.K. Shi Shun, Angew. Chem. Int. Ed. 45 (2006) 1034.
[5] (a) O. Morley, Int. J. Quantum Chem. 46 (1993) 19;
(b) W.J. Buma, M. Fanti, F. Zerbetto, Chem. Phys. Lett. 313 (1999) 426;
(c) J.Y. Lee, S.B. Suh, K.S. Kim, J. Chem. Phys. 112 (2000) 344.
[6] (a) J.B. Armitage, N. Entwistle, E.R.H. Jones, M.C. Whiting, J. Chem. Soc. (1954) 147;
(b) M. Beer, J. Chem. Phys. 25 (1956) 745;
(c) K. Okuyama, T. Hasegawa, M. Ito, N. Mikami, J. Phys. Chem. 88 (1984) 1711;
(d) Y. Hirata, T. Okada, N. Mataga, T. Nomoto, J. Phys. Chem. 96 (1992) 6559;
(e) Y. Hirata, T. Okada, T. Nomoto, Chem. Phys. Lett. 293 (1998) 371;
(f) T. Ishibashi, H. Hamaguchi, J. Phys. Chem. A 102 (1998) 2263;
(g) T. Ishibashi, H. Okamoto, H. Hamaguchi, Chem. Phys. Lett. 325 (2000) 212;
(h) C. Ferrante, U. Kensy, B. Dick, J. Phys. Chem. 97 (1993) 13457;
(i) M. Gutmann, M. Gudipati, P. Schönzart, G. Hohlneicher, J. Phys. Chem. 96 (1992) 2433;
(j) F. Cataldo, O. Ursini, G. Angelini, M. Tommasini, C. Casari, J. Macromol. Sci. Part A 47 (2010) 739.
[7] J.M. Seminario, G.G. Zacarias, J.M. Tour, J. Am. Chem. Soc. 120 (1998) 3970.
[8] A.D. Slepkov, F.A. Hegmann, S.A. Eisler, E. Elliott, R.R. Tykwinski, J. Chem. Phys. 120 (2006) 6807.
[9] S. Anand, O. Varnavski, J.A. Marsden, M.M. Haley, H.B. Schlegel, T. Goodson III, J. Phys. Chem. A 110 (2006) 1305.
[10] Y. Nagano, T. Ikoma, K. Akiyama, S. Tero-Kubota, J. Am. Chem. Soc. 125 (2003) 14103.
[11] M.D. Wahadoszamen, T. Hamada, T. Timori, T. Nakabayashi, N. Ohta, J. Phys. Chem. A 111 (2007) 9544.
[12] M. Pfeiffer, W. Werncke, S. Hogiu, A. Kummrow, A. Lau, Chem. Phys. Lett. 295 (1998) 56.
[13] W.J. Buma, F. Zerbetto, J. Phys. Chem. A 103 (1999) 2220.
[14] J. Catalán, J.L.G. de Paz, J. Chem. Phys. 124 (2006) 034306.
[15] P.O.J. Scherer, S.F. Fischer, J. Photochem. Photobiol. A 145 (2001) 71.
[16] I. Deperasińska, A. Zehnacker, F. Lahmani, P. Borowicz, J. Sepioł, J. Phys. Chem. A 111 (2007) 4252.
[17] R. Dembinski, T. Lis, S. Szafert, C.L. Mayne, T. Bartik, J.A. Gladysz, J. Organomet. Chem. 578 (1999) 229.
[18] M.J. Frisch, G.W. Trucks, H.B. Schlegel, G.E. Scuseria, M.A. Robb, J.R. Cheeseman, V.G. Zakrzewski, J.A. Montgomery Jr., R.E. Stratmann, J.C. Burant, S. Dapprich, J.M. Millam, A.D. Daniels, K.N. Kudin, M.C. Strain, O. Farkas, J. Tomasi, V. Barone, M. Cossi, R. Cammi, B. Mennucci, C. Pomelli, C. Adamo, S. Clifford, J. Ochterski, G.A. Petersson, P.Y. Ayala, Q. Cui, K. Morokuma, D.K. Malick, A.D. Rabuck, K. Raghavachari, J.B. Foresman, J. Cioslowski, J.V. Ortiz, A.G. Baboul, B.B. Stefanov, G. Liu, A. Liashenko, P. Piskorz, I. Komaromi, R. Gomperts, R.L. Martin, D.J. Fox, T. Keith, M.A. Al-Laham, C.Y. Peng, A. Nanayakkara, M. Challacombe, P.M.W. Gill, B. Johnson, W. Chen, M.W. Wong, J.L. Andres, C. Gonzalez, M. Head-Gordon, E.S. Replogle, J.A. Pople, Gaussian 98, Revision A.9, Gaussian, Inc., Pittsburgh, PA, 1998.
[19] R. Ahlrichs, M. Bäar, M. Häser, H. Horn, C. Kölmel, Chem. Phys. Lett. 162 (1998) 165.
[20] R.D. Amos, Chem. Phys. Lett. 364 (2002) 612.
[21] CrysAlisRED Software, Oxford Diffraction, Wrocław, Poland, 1995–2004.
[22] G.M. Sheldrick, Acta Crystallogr., Sect. A 64 (2008) 112.
[23] (a) J. Lewis, B. Lin, M.S. Khan, M.R.A. Al-Mandhary, P.R. Raithby, J. Organomet. Chem. 484 (1994) 161;
(b) G.C.M. Lee, B. Tobias, J.M. Holmes, D.A. Harcourt, M.E. Garst, J. Am. Chem. Soc. 112 (1990) 9330.
[24] (a) K. Osowska, T. Lis, S. Szafert, Eur. J. Org. Chem. (2008) 4598;
(b) M.L. Bell, R.C. Chiechi, C.A. Johnson, D.B. Kimball, A.J. Matzger, W.B. Wan, T.J.R. Weakley, M.M. Haley, Tetrahedron 57 (2001) 3507.
[25] (a) S. Szafert, J.A. Gladysz, Chem. Rev. 103 (2003) 4175;
(b) S. Szafert, J.A. Gladysz, Chem. Rev. 106 (2006) PR1.
[26] B. Bartik, R. Dembinski, T. Bartik, A.M. Arif, J.A. Gladysz, New J. Chem. 21 (1997) 739.
[27] H. Kuhn, J. Chem. Phys. 17 (1949) 1198.
[28] A. Berces, M.Z. Zgierski, in: P. Jensen, P.R. Bunker (Eds.), Computational Molecular Spectroscopy, John Wiley and Sons Ltd., Chichester, 2000, p. 109.
[29] I. Deperasińska, J. Prochorow, Y. Stepanenko, Acta Phys. Pol., A 106 (2004) 535.
[30] L.D. Betowski, M. Enlow, L. Riddick, Comput. Chem. 26 (2002) 317.
[31] M. Parac, S. Grimme, Chem. Phys. 292 (2003) 11.
[32] C. Jamorski, J.B. Foresman, C. Thilgen, H.-P. Lütni, J. Chem. Phys. 116 (2002) 8761.
[33] B.K.V. Hansen, S.V. Hoffman, P.W. Thulstrup, J. Spanget-Larsen, http://www.rub.ruc.dk/dis/chem/psos/2007/DPDA.html.